Longitudinal shear of a composite with elliptic nanofibers: Local stresses and effective stiffness

Kushch, V. I.; Chernobai, V. S.; Mishuris, G. S.

Published in:
International Journal of Engineering Science

DOI:
10.1016/j.ijengsci.2014.06.013

Publication date:
2014

Citation for published version (APA):
Kushch, V. I., Chernobai, V. S., & Mishuris, G. S. (2014). Longitudinal shear of a composite with elliptic nanofibers: Local stresses and effective stiffness. *International Journal of Engineering Science*, *84*, 79-94. https://doi.org/10.1016/j.ijengsci.2014.06.013

Longitudinal shear of elliptic nanofiber composite: local stress and effective stiffness

V.I. Kushch [a] V.S. Chernobai [a] G.S. Mishuris [b]

[a] *Institute for Superhard Materials of the National Academy of Sciences, 04074 Kiev, UKRAINE*

[b] *Institute of Mathematics and Physics, Aberystwyth University, Aberystwyth, SY23 3BZ, U.K.*

Abstract

The paper addresses, for the first time, the problem of calculating the local elastic fields and effective longitudinal shear stiffness of elliptic nano fiber composite with Gurtin-Murdoch interface. The complete, multipole expansion type solutions have been obtained for three most widely used model geometris of fibrous composite, they are single inclusion model, finite cluster model and representative unit cell model. Both the periodic and random microstructure of composite are considered. The developed analytical method combines the superposition principle, the technique of complex potentials and certain new results in the theory of special functions. An appropriate choice of the potentials reduces the the boundary-value problem to an ordinary, well-posed set of linear algebraic equations. This provides an efficient numerical study of the elastic fields and effective stiffness of fibrous nano composite, with the interaction effects adequately taken into account. For the purpose of effective stiffness evaluation, both the Maxwell's and Rayleigh's approaches have been implemented. In the latter case, the exact, closed form formulas for the effective elastic moduli have been derived by analytical averaging the local strain and stress fields. The convergence of solution has been verified and the parametric study of the model problem has been performed. The obtained accurate numerical data illustrate a substantial effect of the inclusion shape and interface elasticity on the local stress concentration and effective elastic behavior of fibrous nano composite.

Key words: nanocomposite, ellipse, Gurtin-Murdoch interface, stress concentration, effective stiffness

Email address: vkushch@bigmir.net (V.I. Kushch).

1 Introduction

The local fields and overall behavior of heterogeneous solids are greatly affected by the interfaces. The assumptions of "perfect interface bonding" or "perfect contact" widely used in micromechanics are not always appropriate. The real-life interfaces are imperfect: the atomic lattices mismatch, poor mechanical or chemical adherence, surface contamination, oxide and interphase diffusion/reaction layers, coatings, interface debonding or cracking, etc. are among the possible reasons of imperfectness. In particular, a distinctive feature of nanostructured materials is experimentally observed (e.g., Miller and Shenoy, 2000; Sharma and Ganti, 2002) dependence of elastic properties on some nano scale length parameter. This dependence is caused by the surface energy and becomes stronger with the interface area to volume ratio increased. For sufficiently high value of this ratio, the interface contribution to local stress field and macroscopic response can be substantial.

To a date, a considerable effort has been made on the continuum description of mechanics of nanomaterials and heterostructures. For the comprehensive review of recent advances in mechanics of nanostructured elements and nanoheterogeneous solids, see Wang et al (2011). The model of elastic surface most often employed in the publications on nanocomposites has been developed by Gurtin and Murdoch (1975, 1978). This model introduces size effect of the surface-related stress, which is an important characteristic of nanocomposites. Specifically, the traction jump across the interface is directly proportional to the residual surface stress and surface elastic properties and inversely proportional to the local radius of curvature. The interface stress jump appears to be extremely small at macro scale (and, therefore, ignored in classical mechanics) but becomes significant at nano scale, typically when the radius of curvature/inhomogeneity is below 100 nm. Based on Gurtin and Murdoch's theory, several authors modified the known micromechanical models by incorporating the surface elasticity feature to include some surface effects in expressions for the effective elastic moduli of nanocomposites (Wang et al, 2011). An effective elastic stiffness of the unidirectional fibrous nanocomposite with coherent interface was studied by means of the generalized self-consistent scheme (Duan et al, 2007a,b) and by the neutral inclusion approach (Chen et al, 2007). The effective inhomogeneity method by Mogilevskaya et al (2010a,b) provides more accurate solution to the homogenization problem by taking into account the interactions among a finite cluster of nanofibers.

Noteworthy, all the above mentioned works dealt with the composites of circular fibers. When the inhomogeneity's shape deviates considerably from the circular one, we need an additional length parameter to quantify it. An elliptical shape providing sufficient flexibility is more appropriate for this purpose. In particular, an infinitely thin elliptic hole is known to be a convenient model of the straight crack. What is important, the curvature radius of elliptic inclusion varies along its surface and may get much smaller values as compared with the circular inclusion of same area. It was mentioned already that the surface effects are inversely proportional to the local radius of curvature, so one can expect their more significant impact on the mechanical behavior of the composite.

To the best of our knowledge, (Luo and Wang, 2009) is the only work where the anti-

plane elastic shear problem for a plane containing a single elliptic nanoinhomogeneity was considered. Despite the importance of the problem, no attempts have been made until now to apply this - or any other - model to the homogenization problem. The main purpose of this work is to develop the micromechanical model of elliptic nanofiber composite providing adequate account of the surface elasticity-induced size effects and interactions between the constituents.

2 Governing equations in terms of complex variables

Longitudinal shear of an aligned fiber composite with isotropic constituents is described by the out-of-plane shear problem of 2D elasticity theory, where u_3 is the only non-zero component of displacement vector $\mathbf{u}$:

$$u_1 = u_2 = 0; \quad u_3 = w(x_1, x_2).$$

In this case, two non-zero components of the stress tensor are σ_{13} and σ_{23}. The stress equilibrium equation $\nabla \cdot \sigma = 0$ takes the form

$$\frac{\partial \sigma_{13}}{\partial x_1} + \frac{\partial \sigma_{23}}{\partial x_2} = 0; \tag{1}$$

the Hooke's law reduces to

$$\sigma_{i3} = 2\mu\varepsilon_{i3} = \mu \partial w/\partial x_i, \quad i = 1, 2. \tag{2}$$

It follows from Eqs (1) and (2) that $\nabla^2 w = 0$ whereas the strain compatibility condition

$$\frac{\partial \varepsilon_{13}}{\partial x_2} = \frac{\partial \varepsilon_{23}}{\partial x_1} = \frac{1}{2}\frac{\partial^2 w}{\partial x_1 \partial x_2}$$

is obeyed identically. This problem is readily reformulated in terms of the complex potentials (Muskhelishvili, 1953). For $w = \mathrm{Re}\,\varphi(z)$, the complex stress $\sigma = \sigma_{13} + \mathrm{i}\sigma_{23} = \mu\overline{\varphi'(z)}$, where $z = x_1 + \mathrm{i}x_2$,

3 Single inclusion in an inhomogeneous far field

3.1 The problem statement

Consider an unbounded plane, or matrix, containing a single elliptic inclusion. All the matrix- and inclusion-related quantities are indexed by "0" and "1", respectively: $w = w^{(0)}$ and $\mu = \mu_0$ in the matrix, $w = w^{(1)}$ and $\mu = \mu_1$ in the inclusion. To describe geometry of the problem, we introduce the Cartesian coordinate frame Ox_1x_2 so that its origin

coincides with the centroid of ellipse whereas the Ox_1 and Ox_2 axes are directed along the major and minor axes of the ellipse. An aspect ratio of the ellipse is $e = l_2/l_1$, where l_1 and l_2 are the major and minor, respectively, semi-axes of the ellipse; its area $S_1 = \pi l_1 l_2$. Another derivative geometric parameter to be used in our analysis is the inter-foci distance $2d$, where $d = \sqrt{l_1^2 - l_2^2}$.

Alongside with conventional complex variable $z = x_1 + \mathrm{i}x_2$, we will use the "elliptic" complex variable $\xi = \zeta + \mathrm{i}\eta$ introduced (e.g., Sneddon and Berry, 1958) as

$$z = d\cosh\xi = \frac{d}{2}(\upsilon + \upsilon^{-1}),\ \upsilon = \exp\xi. \tag{3}$$

In fact, Eq. (3) defines an elliptic coordinate frame with ζ and η as "radial" and "angular" coordinates, respectively. In particular, the coordinate curve $\zeta = \zeta_0$ specified by the condition

$$\zeta_0 = \ln\left(\frac{l_1 + l_2}{d}\right) = \frac{1}{2}\ln\left(\frac{1+e}{1-e}\right) \tag{4}$$

coincides with the boundary of elliptic inclusion. Also, we denote $\upsilon_0 = \exp\zeta_0$. It is important that at this boundary the functions $\upsilon^k = \upsilon_0^k \exp \mathrm{i}k\eta$ depend only on the angular coordinate η. This fact makes the complex variable ξ particularly useful for the domains with elliptic boundaries. In the limiting case of circular ($e = 1$) inclusion, $d \to 0$, $\upsilon_0 \to \infty$, $\upsilon_0 d \to 2R$, $\eta \to \theta$ and $\upsilon d \to 2r\exp \mathrm{i}\theta = 2z$ where r and θ are the circular coordinates. Another limiting case is an infinitely thin ($e = 0$) inclusion or slit/crack where $d = l_1$ and $\upsilon_0 = 1$.

The coherent interface between the matrix and inclusion is assumed in the form of Gurtin-Murdoch's model (e.g., Luo and Wang, 2009):

$$[[\sigma_n]]_L = -\frac{\partial \sigma_t^s}{\partial t};\quad [[w]]_L = 0 \tag{5}$$

where $\sigma_n = 2\mu\nabla w \cdot \mathbf{n} = 2\mu\partial w/\partial n$ is the normal stress and $\sigma_t = 2\mu\nabla w \cdot \mathbf{t} = 2\mu\partial w/\partial t$ is the tangential stress. Here, $[[f]]_L = \left(f^{(0)} - f^{(1)}\right)|_L$ means a jump of quantity f across the interface $L : \zeta = \zeta_0$. Also, $\sigma_t^s = 2\left(\mu^S - \tau^0\right)\varepsilon_t^s$, where μ^S and τ^0 are the surface elastic constants whose dimensionality is $[\mathsf{N/m}]$. In view of the displacement continuity, $\varepsilon_t^s = \partial w_0/\partial t = \partial w_1/\partial t$. To be specific, we take $\sigma_t^s = 2\left(\mu^S - \tau^0\right)\partial w_0/\partial t$. Then, the first interface condition of Eq. (5) yields

$$\left(\widetilde{\mu}_1 \frac{\partial w^{(1)}}{\partial n} - \frac{\partial w^{(0)}}{\partial n}\right)_L = h_c \frac{\partial^2 w_0}{\partial t^2}. \tag{6}$$

where $\widetilde{\mu}_1 = \mu_1/\mu_0$. and $h_c = \frac{\mu^S - \tau^0}{\mu_0}$.

Remark 1 *In the perfect interface case, $\widetilde{\mu}_1$ is the only (bulk property-related) input parameter of the problem. By contrast, here we have an extra input parameter h_c being the*

surface-to-bulk moduli ratio. It has dimensionality [m] *and so can be regarded as a length parameter characterizing the scale behavior of the material. As a consequense, for a finite* $\mu^S - \tau^0$ *a "size effect" is observed, i.e., the elastic fields are dependent on the inclusion size. The available in literature data (e.g., Miller and Shenoy, 2000; Sharma and Ganti, 2002) indicate that* h_c *magnitude is of order of nanometers. Therefore, one can expect the size effect manifestation in heterogeneous solids - including nanocomposites - whose structure length parameter (say, interface curvature) is comparable with* h_c*.*

The displacement field in and outside the inclusion is defined by the far displacement field w_{far}: from the physical consideration, $w^{(0)} \to w_{far}$ when $z \to \infty$. And, to complete the problem formulation, we impose $w^{(1)}(0) = 0$. Our goal is to determine displacement in and outside the inclusion.

3.2 Formal solution

The displacement $w^{(1)}$ is written in terms of the complex potential φ_1 as

$$w^{(1)} = \mathrm{Re}\,\varphi_1, \quad \varphi_1 = \sum_k D_k \upsilon^{-k}, \tag{7}$$

where $D_k = D_{-k}$ (e.g., Muskhelishvili, 1953) due to the fact that $w^{(1)}$ is finite everywhere in the inclusion ($z \in S_1$). Taking $w^{(1)}(0) = 0$ into account yields

$$\varphi_1 = \sum_{k=1}^{\infty} D_k \left(\upsilon^k + \upsilon^{-k}\right). \tag{8}$$

The same reasonings apply to the far displacement field w_{far} assumed to be regular in a vicinity of inclusion, so

$$w_{far} = \mathrm{Re}\,\varphi_{far}, \quad \varphi_{far} = \sum_{k=1}^{\infty} a_k \left(\upsilon^k + \upsilon^{-k}\right). \tag{9}$$

An important particular case is the constant far stress $\sigma_{far} = -\mu_0 E$, where $E = E_1 + \mathrm{i}E_2$. The corresponding displacement $w_{far} = E_1 x_1 + E_2 x_2 = \mathrm{Re}\left(\overline{E}z\right)$. From here, $a_k = \delta_{k1} d\overline{E}/2$, where δ_{ij} is the Kronecker delta.

The total displacement in the matrix $w^{(0)} = w_{far} + w_s$, where w_s is a disturbance due to the inclusion:

$$w^{(0)} = \mathrm{Re}\,\varphi_0, \quad \varphi_0 = \varphi_{far} + \varphi_s. \tag{10}$$

Its asymptotic behavior ($w_s \to 0$ with $z \to \infty$) implies that φ_s series expansion involves only negative powers of υ, i.e.,

$$\varphi_s = \sum_{k=1}^{\infty} A_k \upsilon^{-k}. \tag{11}$$

In what follows, however, we will conveniently write

$$\varphi_0 = \sum_k (A_k + a_k)\, \upsilon^{-k}, \tag{12}$$

where $A_k \equiv 0$ for $k \leq 0$ and $a_k = a_{-k}$.

3.3 Resolving set of equations

The coherent surface (displacement continuity) condition $[[w]]_L = 0$ yields

$$\varphi_1 + \overline{\varphi_1} = \varphi_0 + \overline{\varphi_0}. \tag{13}$$

At the interface L, $\upsilon = \upsilon_0\tau$, where $\tau = \exp i\eta$; hence, $\overline{\upsilon} = \upsilon_0\tau^{-1}$. By substituting φ_1 of Eq.(8) and φ_0 of Eq.(12) into Eq. (13), we get

$$\sum_k D_k\upsilon^{-k} + \sum_k \overline{D_k}\,\overline{\upsilon^{-k}} = \sum_k (A_k + a_k)\, \upsilon^{-k} + \sum_k \left(\overline{A_k} + \overline{a_k}\right) \overline{\upsilon^{-k}}$$

or

$$\sum_k D_k\upsilon_0^{-k}\tau^{-k} + \sum_k \overline{D_{-k}}\upsilon_0^{k}\tau^{-k} = \sum_k (A_k + a_k)\, \upsilon_0^{-k}\tau^{-k} + \sum_k \left(\overline{A_{-k}} + \overline{a_{-k}}\right) \upsilon_0^{k}\tau^{-k}.$$

In view of the orthogonality property of Fourier harmonics $\tau^k = \exp \mathrm{i}k\eta$, we come readily to a set of linear relations

$$D_k\upsilon_0^{-k} + \overline{D_k}\upsilon_0^{k} = (A_k + a_k)\, \upsilon_0^{-k} + \overline{a_k}\upsilon_0^{k} \tag{14}$$

for $k \geq 0$.

In view of the Cauchy-Riemann condition

$$\frac{\partial \operatorname{Re}\varphi}{\partial n} = \frac{\partial \operatorname{Im}\varphi}{\partial t}$$

we get from Eq. (6)

$$\left(\widetilde{\mu}_1 \frac{\partial \operatorname{Im}\varphi_1}{\partial t} - \frac{\partial \operatorname{Im}\varphi_0}{\partial t}\right)_L = h_c \frac{\partial^2 \operatorname{Re}\varphi_0}{\partial t^2}.$$

Now, integration with respect to t along the interface L results in

$$\left(\widetilde{\mu}_1 \operatorname{Im}\varphi_1 - \operatorname{Im}\varphi_0\right)_L = h_c \frac{\partial \operatorname{Re}\varphi_0}{\partial t}.$$

At the elliptic interface $\zeta = \zeta_0$,

$$\frac{\partial\varphi}{\partial n} = \frac{1}{d\sqrt{\sinh^2\zeta_0 + \sin^2\eta}} \frac{\partial\varphi}{\partial\zeta}, \quad \frac{\partial\varphi}{\partial t} = \frac{1}{d\sqrt{\sinh^2\zeta_0 + \sin^2\eta}} \frac{\partial\varphi}{\partial\eta}.$$

So we get

$$\widetilde{\mu}_1 (\varphi_1 - \overline{\varphi_1}) - (\varphi_0 - \overline{\varphi_0}) = \beta \left(\frac{\partial \varphi_0}{\partial \eta} + \overline{\frac{\partial \varphi_0}{\partial \eta}} \right), \tag{15}$$

where

$$\beta = \mathrm{i} \frac{h_c}{l_2} \frac{1}{\sqrt{1 + \alpha \sin^2 \eta}}, \tag{16}$$

$\alpha = \sinh^{-2} \zeta_0$ and $l_2 = d \sinh \zeta_0$ is the minor semi-axis of elliptic inclusion.

Combination of Eq.(15) with Eq.(13) yields

$$(\widetilde{\mu}_1 + 1) \varphi_0 + (\widetilde{\mu}_1 - 1) \overline{\varphi_0} = 2\widetilde{\mu}_1 \varphi_1 + \beta \left(\frac{\partial \varphi_0}{\partial \eta} + \overline{\frac{\partial \varphi_0}{\partial \eta}} \right).$$

In view of Eq.(12) and the obvious identity $\partial \upsilon / \partial \eta = \mathrm{i} \upsilon$, one finds that

$$\begin{aligned} &(\widetilde{\mu}_1 + 1) \sum_n (A_n + a_n) \upsilon^{-n} + (\widetilde{\mu}_1 - 1) \sum_n \left(\overline{A_n} + \overline{a_n} \right) \overline{\upsilon^{-n}} \\ &= 2\widetilde{\mu}_1 \sum_n D_n \upsilon^{-n} + \mathrm{i}\beta \left[\sum_n n (A_n + a_n) \upsilon^{-n} - \sum_n n \left(\overline{A_n} + \overline{a_n} \right) \overline{\upsilon^{-n}} \right]. \end{aligned}$$

Next, we multiply by $\tau^k : k = 1, 2, ...$ and integrate over a period $0 \le \eta \le 2\pi$ to get another infinite set of linear equations:

$$\begin{aligned} &(\widetilde{\mu}_1 + 1) (A_k + a_k) \upsilon_0^{-k} + (\widetilde{\mu}_1 - 1) \overline{a_k} \upsilon_0^k \\ &= 2\widetilde{\mu}_1 D_k \upsilon_0^{-k} + \sum_n n (A_n + a_n) \upsilon_0^{-n} \beta_{k-n} - \sum_n n \left(\overline{A_n} + \overline{a_n} \right) \upsilon_0^{-n} \beta_{k+n}, \end{aligned} \tag{17}$$

where

$$\beta_k = \beta_{-k} = -\frac{\mathrm{i}}{2\pi} \int_L \beta \tau^k d\tau = -\frac{1}{2\pi} \frac{h_c}{l_2} \int_0^{2\pi} \frac{\exp(\mathrm{i}k\eta)}{\sqrt{1 + \alpha \sin^2 \eta}} d\eta. \tag{18}$$

For the recurrent procedure of β_k evaluation, see Appendix A.

The last step is removing the D_k. We express them from Eq.(14) as

$$D_k = \frac{A_k \upsilon_0^{-2k}}{\left(\upsilon_0^{-2k} - \upsilon_0^{2k} \right)} - \frac{\overline{A_k}}{\left(\upsilon_0^{-2k} - \upsilon_0^{2k} \right)} + a_k \tag{19}$$

and substitute into Eq.(17) to get the final form of the linear system:

$$\begin{aligned} &(\widetilde{\mu}_1 + 1) A_k - 2\widetilde{\mu}_1 \left[\frac{A_k \upsilon_0^{-2k}}{\left(\upsilon_0^{-2k} - \upsilon_0^{2k} \right)} - \frac{\overline{A_k}}{\left(\upsilon_0^{-2k} - \upsilon_0^{2k} \right)} \right] + (\widetilde{\mu}_1 - 1) \left(\overline{a_k} \upsilon_0^{2k} - a_k \right) \\ &- \sum_{n=1}^{\infty} n \upsilon_0^{k-n} \left(A_n \beta_{k-n} - \overline{A_n} \beta_{k+n} \right) - \sum_n n \upsilon_0^{k-n} \left(a_n \beta_{k-n} - \overline{a_n} \beta_{k+n} \right) = 0; \\ &k = 1, 2, ... \, . \end{aligned} \tag{20}$$

We mention three degenerate cases of the considered problem, they are (a) perfect interface $\mu^S = \tau^0 = 0$, (b) rigid interface $\mu^S - \tau^0 = \infty$ and (c) circular inclusion, where the solution is elementary (e.g., Mogilevskaya et al, 2010a) and, in the case of uniform far stress, the dipole moment A_1 is the only non-zero expansion coefficient in Eq.(11). A complete solution for a finite $\mu^S - \tau^0$ is given by the infinite series of Eqs (12) and (8) and hence requires an infinite set of linear equations of Eq. (20) to be solved.

$$(1+\widetilde{\mu}_1)\, A_k \upsilon_0^{-k} - 2\widetilde{\mu}_1 \left[\frac{A_k \upsilon_0^{-2k}}{\left(\upsilon_0^{-2k} - \upsilon_0^{2k}\right)} - \frac{\overline{A_k}}{\left(\upsilon_0^{-2k} - \upsilon_0^{2k}\right)} \right] \upsilon_0^{-k} - \sum_{n=1}^{\infty} n \upsilon_0^{-n} \left(A_n \beta_{k-n} - \overline{A_n} \beta_{k+n} \right)$$
$$= \delta_{k1} \frac{d}{2} \left(\widetilde{\mu}_1 - 1\right) \left(\overline{E} \upsilon_0^{-k} - E \upsilon_0^{k} \right) + \frac{d}{2} \overline{E} \left(\upsilon_0^{-1} \beta_{k-1} - \upsilon_0 \beta_{k+1} \right) - \frac{d}{2} E \left(\upsilon_0^{-1} \beta_{k+1} - \upsilon_0 \beta_{k-1} \right).$$

As a consequence, the stress in the inclusion is non-uniform even in the case of uniform far stress.

3.4 Numerical testing

An approximate numerical solution of Eq. (20) up to arbitrary accuracy ε can be found by the truncation method (Kantorovich and Krylov, 1964) which assumes retaining a finite number $n_{\max}(\varepsilon)$ of harmonics in Eq. (11) and the same number of equations in the linear system of Eq. (20). An approximate solution obtained this way tends to exact one as $n_{\max} \to \infty$. In so doing, it is important to keep in mind that convergence rate is substantially affected by the problem parameters. As expected, convergence accelerates when we approach the degenerate cases, i.e., for (a) $h_c \to 0$ and (b) $e = 1$ and arbitrary h_c.

For a finite h_c, the convergence rate slows down when $e \to 0$ and so $n_{\max}$ should be taken sufficiently high to ensure convergent solution. Some idea of the convergence rate can be drawn from the data in Table 1 where the stress $\sigma_{13}^{(0)}(n_{\max})$ on the elliptic hole ($z = l_1$) due to uniaxial far load $\sigma_{13}^{\infty} = 1$ is tabulated. Following Luo and Wang (2009), we take for this and two subsequent examples $h_c = 0.2$ nm and $l_1 = 100$ nm. As seen from the table, for $e = 0.5$ already $n_{\max} = 10$ provides 4-digit accuracy of $\sigma_{13}^{(0)}$ stress value. The same accuracy for $e = 0.05$ and $e = 0.02$ is achieved by retaining in the series Eq. (11) of 150 and 300 harmonics, respectively. In all subsequent numerical tests, $n_{\max}$ was taken so that to ensure convergent (4 digits at least) solution.

Now, we compare our numerical data with those reported by Luo and Wang (2009). In Fig. 1, the stress concentration factor (SCF) $\sigma_{13}(l_1)/\sigma_{13}^{\infty}$ on the matrix ($\sigma_{13} = \sigma_{13}^{(0)}$) and inclusion ($\sigma_{13} = \sigma_{13}^{(1)}$) side of interface is shown as a function of elliptic inclusion long semi-axis l_1. The shear moduli ratio is $\widetilde{\mu}_1 = 0.5$. Our numerical results for $e = 0.2$ and $e = 0.5$ are shown by the solid and dash-dotted curves, respectively. It is clearly seen from the plot that the interface stress jump $[[\sigma_{13}]]$ is size-dependent. As would be expected, it grows up for $l_1 \to 0$ whereas for large l_1 the interface effects become very weak and can be ignored. Also, these data demonstrate that the interface effects are related to the

Table 1
Convergence rate of $\sigma_{23}^{(0)}/\sigma_{23}^{\infty}$ as a function of $n_{\max}$ for $h_c = 0.2$ nm and $a = 100$ nm

	aspect ratio				
nmax	0.5	0.2	0.1	0.05	0.02
10	2.982	5.857	10.46	19.30	44.63
20	2.982	5.820	10.10	17.61	36.94
30		5.815	9.968	16.62	31.64
40		5.814	9.923	16.11	28.36
50		5.814	9.908	15.86	26.36
60			9.904	15.74	25.12
70			9.902	15.68	24.33
80			9.902	15.65	23.83
100				15.63	23.26
150				15.62	22.83
200				15.62	22.74
250					22.72
300					22.71

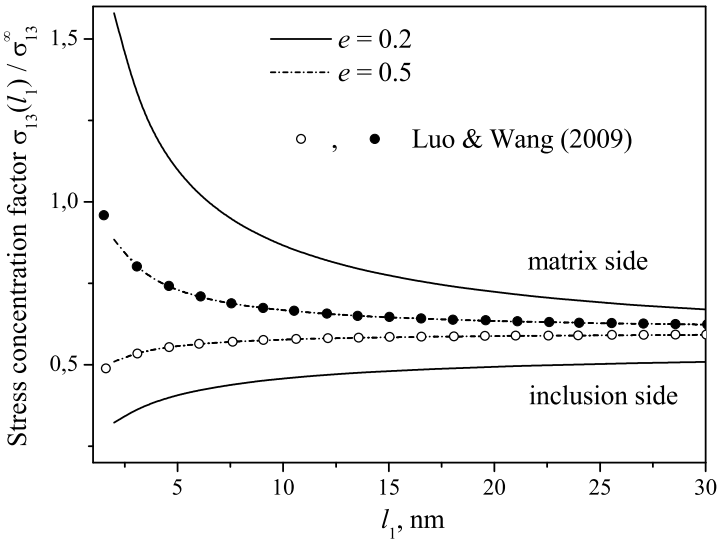

Fig. 1. SCF $\sigma_{13}/\sigma_{13}^{\infty}$ in the point $z = l_1$ as a function of l_1; $\widetilde{\mu}_1 = 0.5$.

local curvature of the interface. For ellipse, the radius of curvature r_c in the point $z = l_1$ equals $(l_2)^2/l_1 = e^2 l_1$. For a fixed l_1 (specifically, $l_1 = 2$ nm) we get $[[\sigma_{13}]]/\sigma_{13}^{\infty} = 0.375$ for $e = 0.5$ and $[[\sigma_{13}]]/\sigma_{13}^{\infty} = 1.258$ for $e = 0.2$. For $e = 0.5$, our data consistent with those

reported by Luo and Wang (2009): the lasts are shown in Fig. 1 by the open ($\sigma_{13}^{(1)}$) and solid ($\sigma_{13}^{(0)}$) circles.

In Fig. 2, the SCF $\sigma_{23}(l_1)/\sigma_{23}^{\infty}$ at the surface of elliptic hole ($\widetilde{\mu}_1 = 0$) is shown as a function of its aspect ratio, e. Again, $l_1 = 100$ nm. For $h_c = 0$ (no surface stress) and $e \to 0$ this stress tends to infinity, in accordance with the linear fracture mechanics. In the limiting case $e = 0$ an ellipse degenerates into straight crack whose tips ($z = \pm d$) produce square root singularity of the stress field, with the corresponding stress intensity factor (SIF) K_{III} defined as

$$\frac{K_{\mathrm{III}}^{\pm}}{\mu_0} = \lim_{z \to \pm d} \sqrt{2\pi\,(z \mp d)}\,\frac{\partial w}{\partial z}.$$

On the contrary, for a finite h_c our computations predicts the finite $\sigma_{23}(l_1)$ limiting value. In this study, $n_{\max}$ varied from several hundreds to a few thousands for $e < 0.01$. Noteworthy, these results are in line with the conclusions made by Kim et al (2010) who studied the nano crack problem (being the limiting case of the problem we consider) numerically, by means of the point wise collocation method. The open and solid circles represent the data by Luo and Wang (2009). The solution for $h_c = 0$ is elementary; for $h_c = 0.2$ as many as 101 harmonics were retained in numerical solution. As seen from Table 1, this $n_{\max}$ value is insufficient in the case of thin ellipse and this is the possible reason of the data deviation for $e < 0.05$.

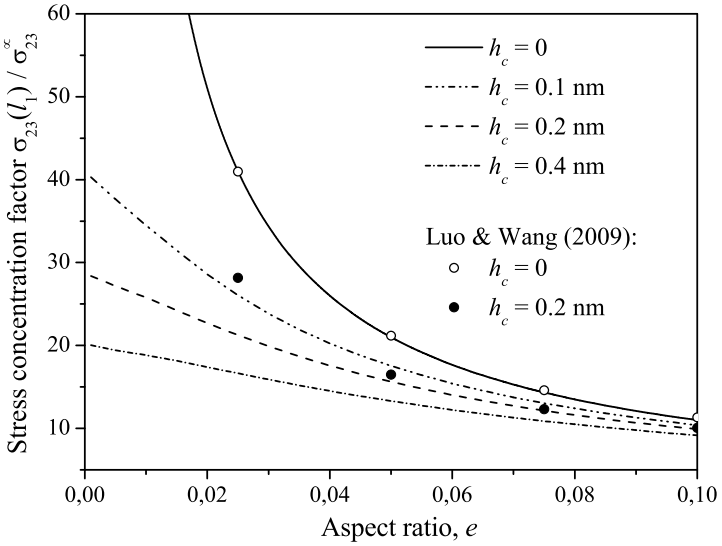

Fig. 2. SCF $\sigma_{23}^{(0)}(l_1)/\sigma_{23}^{\infty}$ at the elliptic hole ($\widetilde{\mu}_1 = 0$) as a function of aspect ratio, e

In the above examples, we prescribed two separate length parameters, both of nanometer scale. They are the characteristic length of material h_c and the inclusion semi-axis length, l_1. In fact, they enter the equations only in the form of the dimensionless number (criterion) being the ratio of these two, see Eq. (16). Introducing this criterion as of a new problem parameter makes our theoretical analysis and numerical results more general. The obvious

Table 2
SCF $\sigma_{23}^{(0)}(l_1)/\sigma_{23}^{\infty}$ at the elliptic hole as a function of aspect ratio e and normalized interface stress $h_c^* = h_c/r_c$

h_c^*	$e = 1.0$	$e = 0.5$	$e = 0.2$	$e = 0.1$	$e = 0.05$	$e = 0.02$
0	2.000	3.000	6.000	11.00	21.00	51.00
0.02	1.961	2.955	5.922	10.86	20.74	50.54
0.05	1.905	2.892	5.814	10.67	20.39	49.87
0.1	1.818	2.796	5.652	10.39	19.85	48.83
0.2	1.667	2.631	5.377	9.902	18.94	46.94
0.5	1.333	2.264	4.778	8.858	16.98	42.48
1.0	1.000	1.866	4.140	7.756	14.92	37.45

definition $\widetilde{h}_c = h_c/l_1$ is not necessarily the best choice: the properly defined criterion is expected to provide useful hint regarding the behavior of material. From this standpoint, the radius of curvature r_c closely related to the surface stress seems to be a good choice for the geometry length parameter. In Table 2, the SCF $\sigma_{23}(l_1)/\sigma_{23}^{\infty}$ at the surface of elliptic hole is shown as a function of its aspect ratio e and normalized interface stress $h_c^* = h_c/r_c$. It is clearly seen from the table that at least for $0.02 \leq e \leq 1$ an effect of surface stress is negligible for $h_c^* << 1$ and significant when h_c^* is of order 1.

4 Multiple inclusion models of composite

The straightforward application of the above theory in the micromechanics is a single inclusion-based (dilute, Maxwell, self-consistent, differential, etc.) scheme for the effective stiffness of elliptic fiber composite with imperfect interface. The Maxwell's homogenization scheme will be discussed in Section 5. In what follows, the solution for a single inclusion is used as the background theory of the advanced models of composite.

4.1 Finite array of inclusions (FCM model)

We consider an elastic plane containing N elliptic nano inclusions. To minimize a number of parameters, we assume all the inclusions to be identical and equally oriented (in x_1 direction). Consideration of composite with inclusions of various size, shape, orientation and properties follows the same way. Thus, geometry of this model is defined by the coordinates (X_{1q}, X_{2q}) of the center O_q of q-th inclusion $(1 \leq q \leq N)$, their aspect ratio $e = l_2/l_1$ and inter foci length $2d$. In literature, this model is also referred as a finite cluster model, or FCM.

Besides the global Cartesian coordinate frame Ox_1x_2, we introduce the inclusion-related

local coordinate frames $O_q x_{1q} x_{2q}$ whose origins coincide with the center of q-th inclusion whereas the $O_q x_{1q}$ and $O_q x_{2q}$ axes are parallel to the corresponding axes of the global coordinate frame. The global $z = x_1 + \mathrm{i}x_2$ and local $z_q = x_{1q} + \mathrm{i}x_{2q}$ variables are related by $z = z_q + Z_q$ ($Z_q = X_{1q} + \mathrm{i}X_{2q}$). The local, inclusion-related elliptic coordinates $\xi_q = \zeta_q + \mathrm{i}\eta_q$ are defined by the formula analogous to Eq. (3):

$$z_q = d\cosh(\xi_q) = \frac{d}{2}(\upsilon_q + \upsilon_q^{-1}),\ \upsilon_q = \exp\xi_q. \tag{21}$$

At the q-th inclusion surface L_q, we have $\zeta_q = \zeta_0$ and $\upsilon_0 = \exp\zeta_0$. The corresponding interface conditions take the form

$$[[\sigma_n]]_{L_q} = -\frac{\partial\sigma_t^s}{\partial t};\quad [[w]]_{L_q} = 0$$

where now $[[f]]_{L_q} = \left(f^{(0)} - f^{(q)}\right)|_{L_q}$. The far field load is given by the displacement $w_{far} = E_1 x_1 + E_2 x_2 = \mathrm{Re}\left(\overline{E}z\right)$.

4.2 Analytical solution

We use the superposition principle to write a general solution of the out-of-plane problem as

$$w^{(0)} = \mathrm{Re}\,\varphi_0,\quad \varphi_0 = \varphi_{far} + \sum_{p=1}^{N}\varphi^{(p)}, \tag{22}$$

where, as before, $\varphi_{far} = \overline{E}z$ is a linear term and

$$\varphi^{(p)} = \sum_{n=1}^{\infty} A_n^{(p)}\widehat{\upsilon}_n(z_p)\quad (1 \le p \le N)\,. \tag{23}$$

In Eq. (23), The functions $\upsilon_n = \upsilon^{-n}$ and $A_n^{(p)}$ are the complex series expansion coefficients to be found.

To fulfil the boundary conditions of Eq. (5), we first expand φ_0 in a vicinity of q-th inclusion (in fact, with respect of its midpoint O_q) into the Laurent series of υ_q. Expansion of the linear term φ_{far} is elementary:

$$\varphi_{far} = \overline{E}Z_q + \frac{\overline{E}d}{2}(\upsilon_q + 1/\upsilon_q).$$

Expansion of the disturbance terms $\varphi^{(p)}$, Eq. (23) employs Eq. (C.2) for the terms with $p = q$ and Eq. (C.5) for the rest of them. Omitting the algebra, we write

$$\varphi_0 = \sum_k \left(A_k^{(q)} + a_k^{(q)}\right)(\upsilon_q)^{-k}\quad (A_k^{(q)} \equiv 0 \text{ for } k \le 0), \tag{24}$$

where

$$a_k^{(q)} = \sum_{p=1}^{N} \sum_{n=1}^{\infty} A_n^{(p)} \eta_{nk}^{pq} + \delta_{k,\pm 1} \frac{\overline{E} d}{2}. \tag{25}$$

The explicit form of the expansion coefficients η_{nk}^{pq} is given by Eq. (B.3). We note also that $a_k^{(q)}$ of Eq. (25) are the expansion coefficients of the regular part of solution and, hence, $a_{-k}^{(q)} = a_k^{(q)}$ is the necessary condition. For more details, see Kushch (2013).

The form of Eq. (24) is the same as of Eq.(12), so the only remaining step is substitution of Eq. (25) into Eq. (20) written for q-th interface. After some algebra, we come to the following compact, convenient for numerical realization formulas:

$$\sum_{n=0}^{\infty} \left(A_n^{(q)} V_{nk}^{(1)} + \overline{A_n^{(q)}} V_{nk}^{(2)} + a_n^{(q)} v_{nk}^{(1)} + \overline{a_n^{(q)}} v_{nk}^{(2)} \right) = 0 \tag{26}$$

$$q = 1, 2, \ ..., N; \quad k = 1, 2, \ ... \ ;$$

where

$$V_{nk}^{(1)} = -n\upsilon_0^{-n} \beta_{k-n} + \delta_{nk} \left[(\widetilde{\mu}_1 + 1) - \frac{2\widetilde{\mu}_1 \upsilon_0^{-2n}}{\upsilon_0^{-2n} - \upsilon_0^{2n}} \right] \upsilon_0^{-n};$$

$$V_{nk}^{(2)} = n\upsilon_0^{-n} \beta_{k+n} + \delta_{nk} \frac{2\widetilde{\mu}_1 \upsilon_0^{-n}}{\upsilon_0^{-2n} - \upsilon_0^{2n}};$$

$$v_{nk}^{(1)} = -n\upsilon_0^{-n} \beta_{k-n} + n\upsilon_0^{n} \beta_{k+n} - \delta_{nk} \left(\widetilde{\mu}_1 - 1 \right) \upsilon_0^{-n};$$

$$v_{nk}^{(2)} = n\upsilon_0^{-n} \beta_{k+n} - n\upsilon_0^{n} \beta_{k-n} + \delta_{nk} \left(\widetilde{\mu}_1 - 1 \right) \upsilon_0^{n}.$$

Numerical solution of the linear system Eq. (26) is obtained by the truncation method.

4.3 RUC model

Now, we consider the representative unit cell (RUC) model of composite with inclusions of elliptic shape. Specifically, we study a composite where the elliptic fibers form a periodic micro structure with the period a along the axes Ox_1 and Ox_2 of the global Cartesian coordinate frame. The unit cell of this material is a square containing N inclusions, see Fig. 3. Within a cell, inclusions are located arbitrarily but without overlapping other inclusions of this and adjacent cells. At the same time, the inclusions can cross the cell boundary: we consider the inclusion as belonging to the cell if the center of inclusion lies inside it. The whole composite bulk is obtained by replicating the unit cell in two orthogonal directions. The volume content of inclusions $c = N\pi l_1 l_2 / a^2$. The random RUC geometry shown in Fig. 3 is generated using the Monte Carlo procedure of Metropolis type (see, e.g., Byström, 2003; Kushch and Chernobai, 2014, for the details).

The strain and stress fields are assumed *macroscopically uniform* and defined by the constant macroscopic gradient E. Due to the cell-type periodicity of geometry, the local

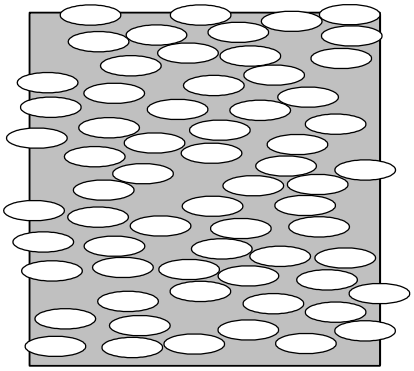

Fig. 3. RUC model of the random structure composite with elliptic fibers: number of inclusions per cell $N = 48$, aspect ratio $e = 1/3$, volume content of inclusions $c = 0.5$.

displacement field is a quasi-periodic function of coordinates:

$$w(z + a) - w(z) = E_1 a; \quad w(z + \mathrm{i}a) - w(z) = E_2 a. \tag{27}$$

Analytical solution of this problem follows the same way as before, with minor modifications. First, the functions $\upsilon_n(z_p)$ Eqs (22) and (23) are replaced with the periodic complex potentials $\widehat{\upsilon}_n(z_p)$ defined by Eq. (C.1) of Appendix C. The properties Eq. (C.4) of the functions $\widehat{\upsilon}_n$ enable fulfilling the periodicity conditions of Eq. (27). Substitution of the modified Eqs (22) and (23) into Eq. (27) gives us

$$\Gamma = E + \frac{\pi d\mathrm{i}}{a^2} \sum_{p=1}^{N} \operatorname{Im} A_1^{(p)}. \tag{28}$$

In view Eq. (28), the modified linear term is $\varphi_{far} = \overline{\Gamma} z$. Also, Γ replaces E in all subsequent equations. The expansion coefficients η_{nk}^{pq} in Eq. (25) are replaced with their periodic counterparts $\eta_{nk}^{*pq} = \eta_{nk}^{pq} + \widetilde{\eta}_{nk}^{pq}$. The explicit form of $\widetilde{\eta}_{nk}^{pq}$ is given by Eq. (B.3), see Kushch (2013) for more details. The linear system of Eq. (26) provides evaluation of the coefficients $A_n^{(p)}$ and thus complete solution of the problem.

5 Effective longitudinal shear stiffness

The general formula for the effective elastic stiffness tensor is $\langle\sigma\rangle = \mathbf{C}^* : \langle\varepsilon\rangle$ where $\langle\varepsilon\rangle$ and $\langle\sigma\rangle$ are the macroscopic strain and stress vector, respectively. In our case, this tensor

formula reduces to two scalar formulas

$$\langle \sigma_{i3} \rangle = 2C^*_{i3j3} \langle \varepsilon_{j3} \rangle = C^*_{i3j3} \left\langle \frac{\partial w}{\partial x_j} \right\rangle, \quad i = 1, 2.$$

To evaluate the effective longitudinal shear stiffness of nanofiber composite, we apply two alternate approaches, both tracing back to the classical works by Maxwell (1873) and Rayleigh (1892).

5.1 Maxwell's approach

Recently, the analytical method has been developed for evaluating the effective conductivity of a composite with the elliptic fibers imperfectly bonded to the matrix Kushch et al (2014a). There, the Maxwell homogenization scheme has been extended to the anisotropic distribution of the inhomogeneities. In the particular case of elliptic fibers, an effective inclusion is the ellipse with aspect ratio governed by the orientation distribution of the individual inhomogeneities. The formula for effective property is derived by equating the induced dipole moment of effective inclusion to the total dipole moment of individual inhomogeneities. In addition to the common (shape of inclusions, their volume content and phase conductivities) structural parameters, this formula accounts also for the interface effects and orientation distribution of fibers. What is important, all the developed in Kushch et al (2014a) theory applies to the problem we considered. To keep things simple, we assume the elliptic inclusions to be equally oriented. In this case, an aspect ratio of effective inclusion is the same as that of actual inclusions Sevostianov (2014). Below, we report briefly the findings of Kushch et al (2014a) and give the working formulas for effective stiffness of composite.

The induced dipole moment of inhomogeneity is commonly defined (e.g., Jackson, 1962) as a parameter governing asymptotic behavior of disturbance field caused by this inhomogeneity. This parameter was de-facto employed by Maxwell to derive his famous formula for the effective stiffness of a composite with spherical particles. In the context of 2-D problem, the complex dipole moment $p = p_1 + \mathrm{i}p_2$ is written in terms of complex variables as (Kushch and Sevostianov, 2013)

$$p = \mu_0 \int_L \left(\frac{\partial w^{(0)}}{\partial n} z - n w^{(0)} \right) \mathrm{d}L, \tag{29}$$

where L is an arbitrary contour encompassing the inhomogeneity and $n = n_1 + \mathrm{i}n_2$ is a complex representation of the unit vector normal to L. In view of Eq. ( ), integration in Eq. (29) is elementary and yields the simple formula for the induced dipole moment p of elliptic inhomogeneity Kushch et al (2014a):

$$p = -\pi d \mu_0 A_1. \tag{30}$$

In the classic Maxwell's homogenization scheme, an equivalent homogeneous inclusion is

a circle of radius R_{eq} and area S_{eq}. The latter is determined by the volume content c of inhomogeneities with area S_1 as

$$S_1 = cS_{eq} = c\pi R_{eq}^2.$$

The isotropic effective stiffness of composite is found as a stiffness μ^* of this equivalent inhomogeneity by equating its dipole moment p_{eq} to the sum p^* of the dipole moments p of individual inhomogeneities inside the representative volume element (RVE) of equal size, S_{eq}. By contrast, the composite of elliptic inhomogeneities we consider is anisotropic at macro level. In the Maxwell homogenization scheme, this anisotropy appears in two ways – as anisotropy of the properties and as anisotropy of the shape of the equivalent inhomogeneity. To calculate effective stiffness using Maxwell homogenization scheme, we equate the dipole moments of elliptic inhomogeneity with imperfect interface to that of equivalent anisotropic inhomogeneity. The last one is also evaluated using Eq. (30).

In the case of aligned ellipses, the effective stiffness of the composite is given by the formulas

$$\frac{C^*_{1313}}{\mu_0} = \frac{(1+\upsilon_0^2)\,P_1 - \upsilon_0^2}{(1-\upsilon_0^2)\,P_1 - \upsilon_0^2}; \quad \frac{C^*_{2323}}{\mu_0} = \frac{(1-\upsilon_0^2)\,P_2 + \upsilon_0^2}{(1+\upsilon_0^2)\,P_2 + \upsilon_0^2}. \tag{31}$$

Here,

$$P_1 + \mathrm{i}P_2 = \frac{\pi dc}{2S_1}\left(\frac{\mathrm{Re}\,A_1}{E_1} + \mathrm{i}\frac{\mathrm{Im}\,A_1}{E_2}\right);$$

where A_1 is found from Eq. (**??**) and $S_1 = \pi l_1 l_2$ is the area of inclusion. As expected, in the particular case of circular nano inclusions of radius R, the composite is macroscopically isotropic ($C^*_{1313} = C^*_{2323} = \mu^*$) and Eq. (31) reduces to that suggested by Chen et al (2007):

$$\frac{\mu^*}{\mu_0} = \frac{(1+c)(\widetilde{\mu}_1 + \widetilde{h}_c) + (1-c)}{(1-c)(\widetilde{\mu}_1 + \widetilde{h}_c) + (1+c)},$$

where $\widetilde{\mu}_1 = \frac{\mu_1}{\mu_0}$ and $\widetilde{h}_c = \frac{\mu^S - \tau^0}{\mu_0 R}$. These parameters enter the formula additively, so the surface effects contribute to the effective stiffness only if $\widetilde{\mu}_1$ and $\widetilde{h}_c$ were of the same order of magnitude.

5.2 Rayleigh's approach

The developed RUC model provides evaluation of the local fields in every point of the unit cell. For our purpose, it is important that these fields can be integrated analytically to obtain the exact, closed form formula for the effective moduli C^*_{i3j3}. Specifically, $\mu^*_{i3} = \langle\sigma_{i3}\rangle$ for $\langle\nabla w\rangle = \mathbf{i}_j$, so we need an explicit expression of the macroscopic gradient and stress corresponding to our displacement solution w, Eqs (22)-(26). The macroscopic quantities $\langle\nabla w\rangle$ and $\langle\sigma\rangle$ are defined as the RVE surface-averaged values of the corresponding local fields (e.g., Zuzovsky and Brenner, 1977; Benveniste and Miloh, 1986):

$$\langle\nabla w\rangle \stackrel{def}{=} \frac{1}{V}\int_S w\mathbf{n}\,\mathrm{d}s, \quad \langle\sigma\rangle \stackrel{def}{=} \frac{1}{V}\int_S (\sigma\cdot\mathbf{n})\,\mathbf{x}\,\mathrm{d}s, \tag{32}$$

where V is a volume and S is a boundary of the representative volume element (RVE) of composite, $\mathbf{x} = x_j \mathbf{i}_j$ is the position vector and $\mathbf{n} = n_j \mathbf{i}_j$ is the normal unit vector. The definition Eq. (32) is advantageous for the following reasons. First, it involves only the observable/measurable quantities - displacement and stress - at the surface of composite specimen. In essence, RVE is considered as a "black box" which makes the definition general, valid for composites with arbitrary interior microstructure. In context of our study, the most important is the fact that, in contrast to the commonly used volume averaging, Eq. (32) holds true for composites with imperfect interfaces. For more discussion on this subject, see Kushch and Sevostianov (2013); Kushch (2013).

Due to macro periodicity of structure imposed by RUC model, the last one can serve as RVE of composite for the effective stiffness evaluation purpose. As would be expected from Eq. (27), $\langle \nabla w \rangle = E_j \mathbf{i}_j$. The formula for average stress in our case becomes

$$\langle \sigma \rangle = -\mu_0 \langle \nabla w \rangle + \frac{1}{a^2} \sum_{q=1}^{N} \mathbf{p}^{(q)}, \tag{33}$$

where

$$\mathbf{p}^{(q)} = \int_{L_q} \left[w^{(0)} \sigma_n (\mathbf{x}) - \sigma_n \left(w^{(0)} \right) \mathbf{x} \right] \mathrm{d}L \tag{34}$$

and L_q is the q-th matrix-inhomogeneity interface. In Eq. (34), integral is taken over the matrix side ($w = w^{(0)}$, $\sigma = \sigma^{(0)}$) of L_q; $\sigma_n (w) = \sigma (w) \cdot \mathbf{n}$ is the normal stress and $\sigma_n (\mathbf{x}) = \sigma_n (x_j) \mathbf{i}_j$. In the considered by us isotropic case, $\sigma_n (\mathbf{x}) = \mu_0 \mathbf{n}$.

In the second term in Eq. (33), $\mathbf{p}^{(q)}$ is the induced dipole moment of q-th inhomogeneity. For further discussion, see Kushch and Sevostianov (2013): here, we note only that the integrals in Eq. (34) involve only the matrix phase displacement field, $w^{(0)}$. Moreover, these integrals are identically zero for all but dipole term in the $w^{(0)}$ multipole expansion in a vicinity of inhomogeneity and represent contribution of these inhomogeneities to the overall stiffness tensor.

Evaluation of the integral of Eq. (34) over the elliptic boundary is ready. In complex variables, it takes the form

$$p^{(q)} = \mu_0 \int_{L_q} \left(\frac{\partial w^{(0)}}{\partial n} z - n w^{(0)} \right) \mathrm{d}L,$$

where $p^{(q)} = p_1^{(q)} + \mathrm{i} p_2^{(q)}$. In view of

$$z = d \cosh \xi, \quad \frac{\partial}{\partial n} = \frac{1}{d \left| \sinh \xi \right|} \frac{\partial}{\partial \zeta}, \quad n = \frac{\sinh \xi}{\left| \sinh \xi \right|}, \quad dL = d \left| \sinh \xi \right| d\eta,$$

Eq. (34) reduces to

$$p^{(q)} = \mu_0 \int_0^{2\pi} \left(\frac{\partial w^{(0)}}{\partial \zeta_q} \cosh \xi_q - w^{(0)} \sinh \xi_q \right) \mathrm{d}\eta_q. \tag{35}$$

Recall that $w^{(0)} = \mathrm{Re}\,\varphi_0$; we substitute the local expansion of φ_0 given by Eq. (24) into Eq. (35). Only zero Fourier harmonics in η_q survives integration over the period, so we get

$$p^{(q)} = -\mu_0 \pi d A_1^{(q)}.$$

As would be expected, only the dipole term contributes to the effective stiffness of composite. Substitution of this expression into Eq. (33) gives the remarkably simple formula

$$\frac{\langle\sigma\rangle}{\mu_0} = E + \frac{\pi d}{a^2}\sum_{q=1}^{N} A_1^{(q)}, \tag{36}$$

consistent with (Kushch and Chernobai, 2014). Together with Eqs. (**??**), re-written as

$$\langle\sigma\rangle = (C^*_{1313} + \mathrm{i}C^*_{2313})E_1 + (C^*_{1323} + \mathrm{i}C^*_{2323})E_2,$$

the formula Eq. (36) provides evaluation of the effective longitudinal shear stiffness of composite.

6 Numerical study

The model we have developed involves a number of parameters contributing to the effective stiffness of composite. They are volume content c of inclusions, their arrangement (Z_q), size and shape (l_1 and l_2), inclusion-to-matrix stiffness ratio $\widetilde{\mu}_1$ and normalized interface stiffness, defined as $\widetilde{h}_c = h_c/l_1$. Also, we limit our consideration by two model geometries of composite. One of them is a periodic orthogonal array whose periods a_1 and a_2 are proportional to inclusion's semi axes: $l_1/a_1 = l_2/a_2$. Another one is the quasi-random geometry shown in Fig. 3. Noteworthy, the last model can be also used to study the periodic structures provided the ratio a_1/a_2 is a rational number, see Fig. 4(?????) for example. An alternate approach consists in considering the rectangle with sides a_1 and a_2 containing one inclusion as a unit cell of periodic composite. All the above theory, with appropriate modification of the standard lattice sums Σ_n^* Eq. (C.7), applies to this model as well. The considered geometries of composite result in macroscopic ortothropy of elastic properties, i.e., $C^*_{1323} = C^*_{2313} = 0$. As to C^*_{1313} and C^*_{2323}, we normalize them by dividing by μ_0 (or, what the same, take $\mu_0 = 1$).

The multiple inclusion model boundary-value problem reduces to an infinite linear system even in the case of perfect interface. Therefore, an accuracy of numerical (approximate, in fact) solution will depend on the number $n_{\max}$ of equations retained in Eq. (26). An accuracy of the reported below numerical data can be estimated from Table 3, where the normalized effective elastic modulus C^*_{1313} of periodic porous solid $\widetilde{\mu}_1 = 0$ is shown as a function of $n_{\max}$ for volume content $c = 0.7$. Computational practice shows that the convergence rate is governed primarily by the volume content of inclusions or, what is the same, by the minimum distance between them. It is seen from the table that for $c = 0.7 \approx 0.9c_{\max}$, where $c_{\max} = \pi/4$ corresponds to dense packing, $n_{\max} = 20$ provides

Table 3
Convergence rate of C^*_{1313} for $c = 0.7$ $\widetilde{\mu}_1 = 0$ (periodic structure)

	$e = 0.5$			$e = 0.2$		
$n_{\max}$	$\widetilde{h}_c = 0$	$\widetilde{h}_c = 0.02$	$\widetilde{h}_c = 0.04$	$\widetilde{h}_c = 0$	$\widetilde{h}_c = 0.02$	$\widetilde{h}_c = 0.04$
1	0,1951	0,2370	0,2785	0,2112	0,3190	0,4238
3	0,1489	0,1990	0,2462	0,1556	0,2760	0,3861
5	0,1420	0,1952	0,244	0,1452	0,2730	0,3852
10	0,1398	0,1945	0,2436	0,1424	0,2727	0,3851
15	0,1397	0,1944	0,2437	0,1422	0,2725	0,3850
20	0,1397	0,1944	0,2437	0,1422	0,2725	0,3850

evaluation of the effective stiffness of composite with at least 4-digit accuracy. What is important in the context of our study, C^*_{1313} convergence rate is practically invariant of h_c.

In Fig. 4, the component C^*_{2323} of the effective stiffness tensor of periodic porous solid is plotted as a function of the volume content of elliptic pores with aspect ratio $e = 0.1$. For the macro level ($\widetilde{h}_c = 0$), the accurate data obtained by the Rayleigh's method (Eq. (36), solid line) coincide up to 4 significant digits with the data by Lu (1994) obtained under assumption of traction-free pore surfaces and shown in the plot by the open circles. The surface stress increases overall stiffness of porous solid: the data obtained from Eq. (36) for $\widetilde{h}_c = 0.1$ are shown by the dashed line. The Maxwell's scheme (Eq. (31), dash-dotted

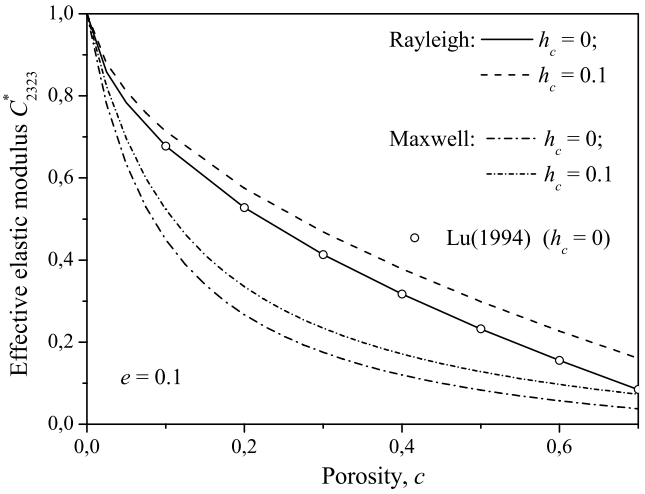

Fig. 4. Effective stiffness C^*_{2323} as a function of porosity (periodic structure)

curves) also predicts growth of C^*_{2323}. however, in both cases it greatly underestimates the macroscopic shear stiffness of porous solid.

The analogous data for effective stiffness C^*_{1313} are plotted in Fig. 5. Again, for $\widetilde{h}_c = 0$ our results coincide with the data reported byLu (1994) whereas Maxwell's scheme overestimates them (dash-dotted curve). It appears that C^*_{1313} is affected by $\widetilde{h}_c$ much

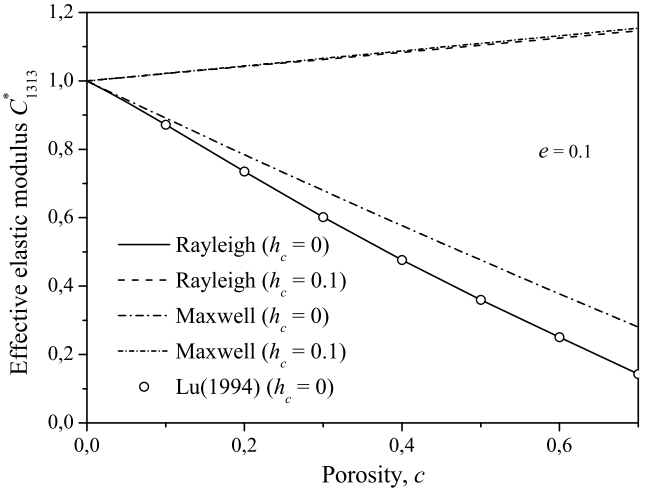

Fig. 5. Effective stiffness C^*_{1313} as a function of porosity c (periodic structure)

more substantially than μ^*_{23} and for $\widetilde{h}_c = 0.1$ the effective stiffness μ^*_{13} of porous solid *exceeds* that of a bulk material, μ_0. Interestingly, in the last case prediction made by the Rayleigh's and Maxwell's methods are very close. These examples clearly demonstrate that the interfaces affect the overall stiffness of nanostructured materials quite substantially and therefore must be taken into account.

In Fig. 6, the effective elastic moduli C^*_{1313} and C^*_{2323} of porous solid with $c = 0.5$ are shown as dependent of $\widetilde{h}_c$. As would be expected, for $e = 1$ (circular pores) $C^*_{1313} = C^*_{2323}$ and is a weakly growing function of $\widetilde{h}_c$ shown in the plot by the dash-dotted curve and open circles. For $e < 1$, $C^*_{2323}(e) < C^*_{2323}(1)$ whereas $C^*_{1313}(e) > C^*_{1313}(1)$ and their difference is getting bigger as $e \to 0$. For example, an anisotropy parameter C^*_{1313}/C^*_{2323} equals 1.38 for $e = 0.5$ and 2.33 for $e = 0.2$.

To complete this part, we give two examples of the surface effects in the periodic and random composites with $c = 0.5$ and $e = 1/3$. The random structure was modeled by RUC with $N = 48$ equally oriented inclusions per cell (Fig. 3). The effective moduli of random composite were obtained by averaging the output data over 20 runs. In Table 4, the effective moduli $C^*_{1313}(\widetilde{h}_c)$ and $C^*_{2323}(\widetilde{h}_c)$ are shown as a function of $0 \le \widetilde{\mu}_1 \le 10$ for $\widetilde{h}_c = 0$ and $\widetilde{h}_c = 0.2$. The last value is intentionally taken sufficiently large to illustrate an effect of $\widetilde{h}_c$. Noteworthy, C^*_{i3i3} are the nearly linear functions of $\widetilde{h}_c$, so one can estimate their values for $0 < \widetilde{h}_c < 0.2$ based on the tabulated data. As seen from the table, an effect of $\widetilde{h}_c$ is the most prominent for $\widetilde{\mu}_1 \le 1$ whereas for $\widetilde{\mu}_1 = 1$ the difference between $C^*_{1313}(0.2)$ and $C^*_{1313}(0)$ is below 2% for C^*_{1313} and below 1% for C^*_{2323}.

In Fig. 7, the effective modulus C^*_{1313} is shown as a function of $\widetilde{\mu}_1$ for $\widetilde{h}_c = 0$ and $\widetilde{h}_c = 0.2$.

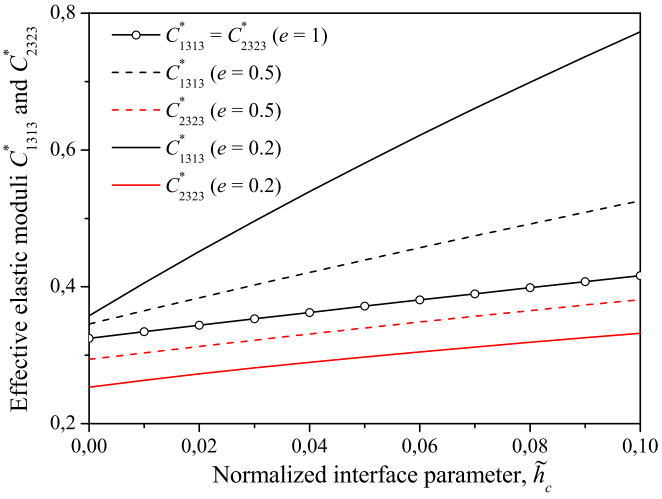

Fig. 6. Effective elastic moduli C^*_{1313} and C^*_{2323} of porous solid with $c = 0.5$ as the functions of $\widetilde{h}_c$

Table 4
The effective elastic moduli $C^*_{1313}(\widetilde{h}_c)$ and $C^*_{2323}(\widetilde{h}_c)$ of periodic and random composite with $c = 0.5$ and $e = 1/3$

	periodic structure				random structure			
$\widetilde{\mu}_1$	$C^*_{1313}(0)$	$C^*_{2323}(0)$	$C^*_{1313}(0,2)$	$C^*_{2323}(0,2)$	$C^*_{1313}(0)$	$C^*_{2323}(0)$	$C^*_{1313}(0,2)$	$C^*_{2323}(0,2)$
0,0	0,353	0,275	0,835	0,427	0,368	0,143	0,845	0,341
0,25	0,552	0,515	0,975	0,628	0,575	0.466	0,977	0,594
0,5	0,720	0,706	1,100	0,796	0,731	0,690	1,100	0,785
0,75	0,868	0,865	1,212	0,939	0,871	0,862	1,216	0,937
1,0	1,0	1,0	1,314	1,062	1,0	1,0	1,326	1,062
2,0	1,417	1,388	1,646	1,424	1,45	1,369	1,722	1,404
4,0	1,946	1,818	2,085	1,829	2,141	1,741	2,335	1,756
6,0	2,271	2,041	2,364	2,052	2,646	1,940	2,810	1,948
8,0	2,491	2,186	2,557	2,194	3,070	2,073	3,214	2,080
10,0	2,650	2,287	2,700	2,292	3,484	2,128	3,567	2,141

The data for periodic and random composite are shown in black and red, respectively. The blue curves represents the Maxwell's scheme. It is seen that for $0 \leq \widetilde{\mu}_1 < 2$ the predictions of all three models are pretty close and predict the same effective stiffness growth due to $\widetilde{h}_c$. For $\widetilde{\mu}_1 > 2$, an effect of $\widetilde{h}_c$ decreases and micro structure becomes a dominant factor. The crossed open circles in Fig. 7 represent the data by Byström (2003) for $\widetilde{\mu}_1 = 10$ who studied the analogous models numerically and found $C^*_{1313} = 2.650$ for

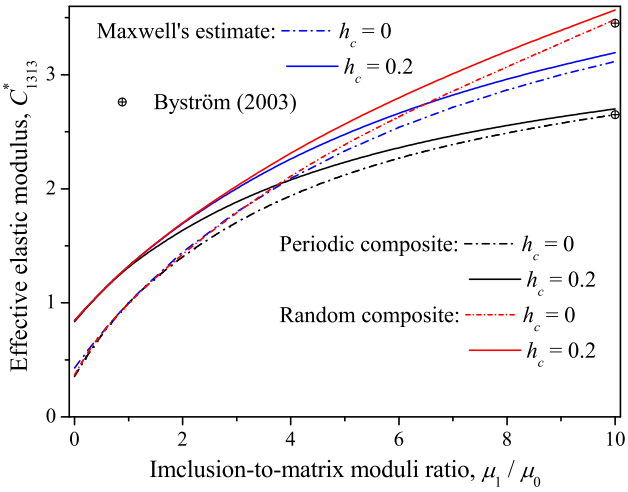

Fig. 7. Effective elsticc modulus C^*_{1313} as a function of $\widetilde{\mu}_1$ for $\widetilde{h}_c = 0$ and $\widetilde{h}_c = 0, 2$.

periodic and $C^*_{1313} = 3.452$ for random composite. Our method predicts $C^*_{1313} = 2.650$ and $C^*_{1313} = 3.484$ for the periodic and random composite with $\widetilde{\mu}_1 = 10$ and $h_c = 0$ (no interface effect), respectively, see Table 4. These numbers within $0,1\%$ agree with those reported by Byström (2003). Such a good correlation can be regarded as the correctness proof and accuracy validation of the developed method and numerical algorithms.

7 Conclusions

The analytical, multipole expansion method has been developed to study the elastic behavior of composite with aligned, elliptic in cross-section nanofibers due to longitudinal shear. For the first time, a complete solution has been obtained for the FCM and RUC models of fibrous nanocomposite with Gurtin-Murdoch type interface. Both the periodic and random microstructure of composite are considered. In the latter case, the representative unit cell of a composite contains multiple elliptic inclusions. The method combines the principle of superposition, technique of complex potentials and some new results in the theory of special functions. An appropriate choice of complex potentials and the re-expansion formulas for them reduce the boundary-value problem for a heterogeneous solid to an ordinary, well-posed set of linear algebraic equations. This in turn reduces the computational effort of solution greatly and thus provides an efficient numerical study of the elastic fields and effective stiffness of fibrous nano composite, with the interaction effects adequately taken into account.

The homogenization problem for a composite containing elliptic nano inclusions never been considered even approximately so the theory has been developed and numerical estimates of the effective stiffness of composites with finite characteristic length parameter h_c have been obtained for the first time. For this purpose, both the Maxwell's and Rayleigh's

approaches have been implemented. In the latter case, the exact finite form expressions of the effective elastic moduli have been derived by analytical averaging of the local strain and stress fields. The reported in the paper accurate numerical data illustrate substantial effect of interface elasticity and related size effect on the local stress concentration and effective stiffness of composite. In particular, the surface effect makes the stress field in the inclusion non-uniform even in the Eshelby's problem and gives a rise to size-dependence of the stress concentration factor. The stress in the tip of infinitely thin elliptic nano cavity is finite, in contrast to the traction-free surface case. The effective stiffness of composite is also affected by the surface/interface effects and the inclusion's shape. Their combined action results in (a) macroscopic anisotropy of elastic properties and (b) manifestation of the surface elasticity effects in composite with coarser inclusions as compared with the circular fiber case. The latter is due to the fact that traction jump across the interface in Gurtin-Murdoch model is inversely proportional to the local radius of curvature. The general conclusion drawn from our numerical study is that elastic stiffness and brittle strength of nanoheterogeneous materials can be substantially improved by appropriate choice of inclusion shape and modification of interfaces. The developed semi-analytical technique, able to accurately evaluate the elastic fields of interacting nanoinhomogeneities, opens new opportunities in computer-aided design of new nanostructured materials with tailor-made mechanical properties.

Acknowledgements

The authors gratefully acknowledge the support from the FP7 IRSES project TAMER IRSES-GA-2013-610547.

A Evaluation of β_k coefficients

We re-write Eq. (18) as

$$\beta_k = -\frac{1}{2\pi}\frac{h_c}{l_2}\int_0^{2\pi}\frac{\cos k\eta - \mathrm{i}\sin k\eta}{\Delta(\alpha)}\mathrm{d}\eta.$$

where $\Delta(\alpha) = \sqrt{1+\alpha\sin^2\eta}$. It is readily seen that for all integer k

$$\int_0^{2\pi}\frac{\sin k\eta}{\Delta(\alpha)}\mathrm{d}\eta \equiv 0; \quad \int_0^{2\pi}\frac{\cos\left(2k+1\right)\eta}{\Delta(\alpha)}\mathrm{d}\eta \equiv 0;$$

so we only need to evaluate the integrals of type

$$I_k = \int_0^{2\pi}\frac{\cos 2k\eta}{\Delta(\alpha)}\mathrm{d}\eta = 4\int_0^{\pi/2}\frac{\cos 2k\eta}{\Delta(\alpha)}\mathrm{d}\eta. \tag{A.1}$$

For $k = 0$ and $k = 1$, these integrals are written in terms of complete elliptic integrals of the first and second kind, defined as (Abramovitz and Stegun, 1964)

$$\mathsf{K}(\alpha) = \int_0^{\pi/2} \frac{\mathrm{d}x}{\Delta(-\alpha)} \quad \text{and} \quad \mathsf{E}(\alpha) = \int_0^{\pi/2} \Delta(-\alpha)\mathrm{d}x,$$

respectively. By comparison with Eq. (A.1), one finds

$$I_0 = 4\sqrt{\alpha}\mathsf{K}(-\alpha) \tag{A.2}$$

and

$$I_1 = 4\sqrt{\alpha}\left[\left(1 + \frac{2}{\alpha}\right)\mathsf{K}(-\alpha) - \frac{2}{a}\mathsf{E}(-\alpha)\right]. \tag{A.3}$$

Now, we derive the recurrent formula for I_k, $k \geq 2$. The standard trigonometry consideration yields

$$\frac{I_{k+1}}{\sqrt{\alpha}} = \int_0^{2\pi} \frac{\cos 2k\eta \cos 2\eta}{\Delta(\alpha)}\mathrm{d}\eta - \int_0^{2\pi} \frac{\sin 2k\eta \sin 2\eta}{\Delta(\alpha)}\mathrm{d}\eta \tag{A.4}$$

and

$$\int_0^{2\pi} \frac{\cos 2k\eta \cos 2\eta}{\Delta(\alpha)}\mathrm{d}\eta = \frac{I_{k+1} + I_{k-1}}{2\sqrt{\alpha}}.$$

Also, we apply the differentiation formulas

$$\frac{2}{a}\mathrm{d}\Delta(\alpha) = \frac{\sin 2\eta \mathrm{d}\eta}{\Delta(\alpha)}; \quad \mathrm{d}\sin 2k\eta = 2k\cos 2k\eta \mathrm{d}\eta;$$

and integration by parts to transform the second integral in Eq. (A.4):

$$\begin{aligned}
&\int_0^{2\pi} \frac{\sin 2k\eta \sin 2\eta}{\Delta(\alpha)}\mathrm{d}\eta = \frac{2}{\alpha}\int_0^{2\pi} \sin 2k\eta \ \mathrm{d}\Delta(\alpha) \\
&= \frac{2}{\alpha}\left[\sin 2k\eta \ \mathrm{d}\Delta(\alpha)^{1/2}\Big|_0^{2\pi} - \int_0^{2\pi} \Delta(\alpha)\mathrm{d}\sin 2k\eta\right] \\
&= -2k\left(\frac{2}{\alpha} + 1\right)\frac{I_k}{\sqrt{\alpha}} + 2k\int_0^{2\pi} \frac{\cos 2k\eta \cos 2\eta}{\Delta(\alpha)}\mathrm{d}\eta
\end{aligned}$$

By combining the above formulas, we obtain the recurrent formula

$$\left(\frac{1}{2} + k\right) I_{k+1} = \left(\frac{1}{2} - k\right) I_{k-1} + 2k\left(\frac{2}{\alpha} + 1\right) I_k. \tag{A.5}$$

Together with Eqs (A.2) and (A.3), Eq. (A.5) provides an efficient evaluation of I_k and hence β_k coefficients of Eq. (18).

B Re-expansion formulas for the elliptic solid harmonics

The series expansion of the p-th inclusion-related irregular elliptic harmonics $(\upsilon_p)^{-n}$ $(n > 0)$ in a vicinity of another, q-th inclusion is given by the formula (Kushch et al., 2005)

$$\upsilon_p^{-n} = \sum_{m=0}^{\infty} \eta_{nm}^{pq} \left(\upsilon_q^m + \upsilon_q^{-m} \right) \quad (n \geq 1)\,; \tag{B.1}$$

where the expansion coefficients $\eta_{nm}^{pq} = \eta_{nm}\left(Z_{pq}, d_p, d_q\right)$ and $Z_{pq} = Z_q - Z_p$. For the arbitrarily located, equally oriented elliptic coordinate frames $O_p x_{1p} x_{2p}$ and $O_q x_{1q} x_{2q}$ with the same semi-foci parameter $d_p = d_q = d$, Yardley et al (1999) have suggested the formula

$$\eta_{nm}(Z_{pq}) = \frac{1}{\pi} \int_0^{\pi} (\upsilon_p)^{-n} \Big|_{\zeta_q = 0} \cos(m\eta_q) d\eta_p. \tag{B.2}$$

Computational effort of η_{nm} evaluation from (B.2) is quite considerable. An efficiency of numerical algorithm can be improved by using two series expansions of η_{nm} (Kushch et al., 2005). The first one is

$$\begin{aligned} \eta_{nm}(Z) = (-1)^m n \sum_{j=0}^{\infty} V^{-(n+m+2j)} \\ \times \sum_{l=0}^{j} \frac{(-1)^{j-l}}{(j-l)!} \left(\frac{1}{2}\right)^{n+m+2l} M_{nml} \frac{(n+m+l+j-1)!}{(j-l)!}. \end{aligned} \tag{B.3}$$

where V is defined by $Z = d\left(V + V^{-1}\right)$. Here,

$$M_{nml} = \frac{(n+m+l+1)_l}{l!\,(n+l)!\,(m+l)!},$$

where $(n)_m$ is the Pohgammer's symbol. The series Eq. (B.1) with the coefficients Eq. (B.3) converges within an ellipse centered in Z_q with inter-foci distance $2d$ and passing the pole of p-th elliptic coordinate frame closest to Z_q which is sufficient to solve for any two non-overlapping ellipses. For the well-separated (namely, $|z_p| > d$, $|z_q| < |Z_{pq}|$ and $|Z_{pq}| > 2d$) inclusions, Eq. (B.3) simplifies to

$$\eta_{nm}(Z) = n\,(-1)^m \sum_{l=0}^{\infty} d^{2l+n+m} M_{nml} \frac{\Gamma\left(n+m+2l\right)}{(2Z)^{n+m+2l}}. \tag{B.4}$$

C Periodic complex potentials

Following Kushch et al. (2009b), we define the functions $\widehat{\upsilon}_n$ as 2D lattice sums:

$$\widehat{\upsilon}_n(z) = \sum_{\mathbf{k}} \left[\upsilon(z + W_{\mathbf{k}})\right]^{-n} \quad (n \geq 1)\,, \tag{C.1}$$

where $W_{\mathbf{k}} = a\mathbf{k} = a\,(k_1 + \mathrm{i}k_2)$, $-\infty < k_1, k_2 < \infty$. The drawback of this definition is the convergence issue: in fact, the series Eq. (C.1) for $n = 1$ is conditionally convergent (Kushch, 2013). An alternate way of defining the functions $\widehat{v}_n$ uses their local series expansion of the form

$$\widehat{v}_n = v^{-n} + \sum_k \widetilde{\eta}_{nk}(0)\,(v)^{-k}\,, \tag{C.2}$$

where

$$\widetilde{\eta}_{nk}(z) = \sum_{\mathbf{k}\neq\mathbf{0}} \eta_{nm}\,(z + W_{\mathbf{k}})\,, \tag{C.3}$$

η_{nm} being the re-expansion coefficient defined by Eq. (B.1). For $n > 1$, the definitions by Eqs (C.1) and (C.2) are equivalent. The periodic harmonics introduced this way obey the following periodicity conditions:

$$\begin{aligned} \widehat{v}_n(z + a) - \widehat{v}_n(z) &= 0; \\ \widehat{v}_n(z + \mathrm{i}a) - \widehat{v}_n(z) &= \delta_{n1}\frac{\pi d\mathrm{i}}{a}; \end{aligned} \tag{C.4}$$

and possess a countable set of cuts centered in the points $W_{\mathbf{k}}$. The series Eq. (C.1) is termwise differentiable which means that $\widehat{v}_n$ obeys Laplace equation and can be thought as the periodic complex potential.

In order to fulfil the boundary conditions at the q-th inclusion, we need the local expansion of $\widehat{v}_n(z_p)$ in terms of v_q. This regular expansion is readily derived with aid of the re-expansion formulas Eq. (B.1). We write it in the following form

$$\widehat{v}_n(z_p) = \sum_m \left(\eta_{nm}^{pq} + \widetilde{\eta}_{nm}^{pq}\right)(v_q)^{-m}\,, \tag{C.5}$$

where $\widetilde{\eta}_{nm}^{pq} = \widetilde{\eta}_{nk}(Z_{pq})$ and $\widetilde{\eta}_{nm}^{pq} = \widetilde{\eta}_{nk}(Z_{pq})$. In Eq. (C.5), Z_{pq} is understood as a minimum distance between the p-th and q-th inclusions, with account for those belonging to the adjacent cells: $Z_{pq} = \min(Z_q - Z_p \pm a \pm \mathrm{i}a)$. Then, the first term in Eq. (C.5) is computed using Eq. (B.3). As to the second one, given by Eq. (C.6), we note that $a \gg d$ for the typical RUC model. Therefore, Eq. (B.4) applies here and so we get

$$\widetilde{\eta}_{nm}^{pq} = n\,(-1)^m \sum_{l=0}^{\infty} \left(\frac{d}{2}\right)^{n+m+2l} M_{nml}\Gamma\,(n + m + 2l)\,\Sigma^*_{n+m+2l}(Z_{pq}), \tag{C.6}$$

where Σ_n^* is the standard lattice sum defined as

$$\Sigma_n^*(z) = \sum_{\mathbf{k}\neq 0} (z + W_{\mathbf{k}})^{-n}\,. \tag{C.7}$$

References

Abramovitz, M., Stegun, I.A., 1964. Handbook for mathematical functions. NBS Applied Mathematics Series, vol. 55. Flammarion.

Benveniste, Y., Miloh, T., 1986. The effective stiffness of composites with imperfect thermal contact at constituent interfaces. Int. J. Eng. Sci., 24, 1537–1552.

Byström, J., 2003. Influence of the inclusions distribution on the effective properties of heterogeneous media. Composites: Part B, 34, 587–592.

Chen,T., Dvorak,G.J. and Yu,C.C., Size-dependent elastic properties of unidirectional nano-composites with interface stresses. Acta Mechanica, 2007, 188: 39-54.

Duan,H.L., Yi,X., Huang,Z.P. and Wang,J., A unified scheme for prediction of effective moduli of multiphase composites with interface effects: Part I — theoretical framework. Mechanics of Materials, 2007a,39: 81-93.

Duan,H.L., Yi,X., Huang,Z.P. and Wang,J., A unified scheme for prediction of effective moduli of multiphase composites with interface effects: Part II — application and scaling laws. Mechanics of Materials, 2007b, 39: 94-103.

Gurtin, M.E., Murdoch, A.I., 1975. A continuum theory of elastic material surfaces. Arch. Ration. Mech. Anal. 57, 291–323.

Gurtin, M.E., Murdoch, A.I., 1978. Surface stress in solids. Int. J. Solids Struct. 14, 431–440.

Jackson, J.D. (1962). Classical Electrodynamics. Wiley.

Kantorovich, L.V., Krylov, V.I., 1964. Approximate Methods of Higher Analysis. Wiley, New York.

Kim, C.I., Schiavone, P., Ru, C.-Q., 2010. The effects of surface elasticity on an elastic solid with mode-III crack: complete solution. ASME Journal of Applied Mechanics, 77, 021011-1/7.

Kushch, V.I., Shmegera, S.V., Buryachenko, V.A. (2005). Interacting elliptic inclusions by the method of complex potentials. International Journal of Solids and Structures 42, 5491–5512

Kushch, V.I., Sevostianov, I., Mishnaevsky, L. Jr, 2009. Effect of crack orientation statistics on effective stiffness of mircocracked solid. Int. J. Solids Struct., 46, 1574–1588.

Kushch, V.I. (2013). Micromechanics of composites: multipole expansion approach. Elsevier.

Kushch, V.I., Sevostianov, I. (2013). Dipole moments, property contribution tensors and effective stiffness of anisotropic particulate composites. International Journal of Engineering Science 74, 15–34.

Kushch, V.I., Chernobai, V.S. (2014). Transverse stiffness and longitudial shear of elliptic fiber composite with imperfect interface (submitted).

Kushch, V.I., Sevostianov, I., & Chernobai, V.S. (2014a). Effective conductivity of composite with imperfect contact between elliptic fibers and matrix: Maxwell's homogenization scheme (submitted).

Lu, S.-Y. (1994). Anisotropy in effective conductivities of rectangular arrays of elliptic cylinders. Journal of Applied Physics, 76, 2641–2647.

Luo, J., Wang, X. (2009). On the anti-plane shear of an elliptic nano inhomogeneity. European Journal of Mechanics A/Solids, 28, 926–934.

Maxwell, J.C. (1873). A Treatise on Electricity and Magnetism. Vol. 1. Clarendon Press.

Miller, R.E., Shenoy, V.B., 2000. Size-dependent elastic properties of nanosized structural elements. Nanotechnology 11, 139–147.

Mogilevskaya,S.G., Crouch,S.L., La Grotta,A. and Stolarski,H.K., The effects of surface

elasticity and surface tension on the transverse overall elastic behavior of unidirectional nanocomposites. Composites Science and Technology, 2010a, 70: 427-434.

Mogilevskaya,S.G., Crouch,S.L., Stolarski,H.K. and Benusiglio,A., Equivalent inhomogeneity method for evaluating the effective elastic properties of unidirectional multiphase composites with surface/interface effects. International Journal of Solids and Structures, 2010b, 47: 407-418.

Muskhelishvili, N.I., 1953. Some basic problems of the mathematical theory of elasticity. Groningen, P. Noordhoff.

Rayleigh, Lord, 1892. On the influence of obstacles arranged in rectangular order on the properties of a medium. Philos. Mag., E34, 481–502.

Sevostianov, I. (2014). On the shape of efective inclusion in the Maxwell homogenization scheme for anisotropic elastic composites, Mechanics of Materials (under review).

Sharma, P., Ganti, S., 2002. Interfacial elasticity corrections to size-dependent strain-state of embedded quantum dots. Phys. Stat. Sol. 234, R10-R12.

Sneddon, I.N., & Berry, D.S. (1958). The classical theory of elasticity. Springer.

Wang, J., Huang, Z., Duan, H., Yu, S., Feng, X., Wang, G., Zhang, W., Wang, T., 2011. Surface stress effect in mechanics of nanostructured materials. Acta Mechanica Solida Sinica, 24, 52–82.

Yardley, R.C., McPhedran, J.G., & Nicorovici, N.A. (1999). Addition formulas and the Rayleigh identity for arrays of elliptical cylinders. Physical Reviw E 60, 6068–6080.

Zuzovsky, M., Brenner, H., 1977. Effective conductivities of composite materials composed of cubic arrangements of spherical particles embedded in an isotropic matrix. Z. Agnew. Math. Phys. (ZAMP), 28, 979–992.